Geochemical Characteristics of Surface Sediments in the Xunmei Hydrothermal Field (26°S), Mid-Atlantic Ridge: Implications for Hydrothermal Activity

Peng Yang *, Chuanshun Li *, Yuan Dang *, Lei Fan , Baoju Yang , Yili Guan , Qiukui Zhao , Dewen Du

Posted Date: 15 August 2023

doi: 10.20944/preprints202308.1072.v1

Keywords: South Mid-Atlantic Ridge; metalliferous sediments; Xunmei Hydrothermal Field; geochemical characteristics

Article

Geochemical Characteristics of Surface Sediments in the Xunmei Hydrothermal Field (26°S), Mid-Atlantic Ridge: Implications for Hydrothermal Activity

Peng Yang [1], Chuanshun Li [1,2]*, Yuan Dang [1,2,*], Lei Fan [1,2], Baoju Yang [3], Yili Guan [1,2], Qiukui Zhao [4] and Dewen Du [1,2]

[1] Key Laboratory of Marine Geology and Metallogeny, First Institute of Oceanography, Ministry of Natural Resources, Qingdao 266061, China
[2] Shandong Key Laboratory of Deep Sea Mineral Resources Development, Qingdao 266061, China
[3] School of Resources and Environmental Engineering, Ludong University, Yantai 264025, China
[4] College of Marine Geosciences, Ocean University of China, Qingdao 266100, China
* Correspondence: lichuanshun@fio.org.cn; dangyuan@fio.org.cn

Abstract: The compositions of metalliferous sediments which is associated with hydrothermal vents can provide reliable geochemical indicators for the exploration of seafloor sulfides. In this study, surface sediments from the Xunmei hydrothermal field (HF) on the South Mid-Atlantic Ridge (SMAR) were selected, and their major and trace elements were analysed. The results showed that the sediments are composed of pelagic material (calcium biogenic components), basaltic debris, iron-manganese oxides, and a mixture of hydrothermal components. Additionally, the sediments were found to be significantly enriched in Cu, Zn, Fe and Co derived from hydrothermal sources, as well as Mn, V, Mo, U and P, which are primarily scavenged from seawater. The Cu and Zn concentrations are highest in the northeastern part of Xunmei, while the northeastern, northern, and southern parts are characterized by great inputs of hydrothermal Fe. Manganese and Mo are mainly enriched in the western and southern parts and show a strong positive correlation, indicating that Mo is mainly scavenged by Mn oxides. There are high positive correlations among U, P, and Fe, indicating their coprecipitation with Fe from hydrothermal plumes. Vanadium and Co are introduced into sediments in two ways, i.e., V is scavenged and coprecipitates from hydrothermal plumes, and Co is derived from sulfide debris. Based on the variations in Cu and Zn contents and in the Cu/Fe (0.159), Zn/Fe (0.158), and Fe/Mn (1440) ratios, it can be inferred that a high-temperature hydrothermal vent existed in northeastern Xunmei. In combination with the distribution patterns of the above elements, the hydrothermal vents in the southern part ceased erupting after a short period of activity. In addition, the high Mn anomaly and the high U/Fe ratios at the boundaries of the investigated area indicate the presence of a relatively oxidized environment in southwestern Xunmei.

Keywords: South Mid-Atlantic Ridge; metalliferous sediments; Xunmei Hydrothermal Field; geochemical characteristics

1. Introduction

The global modern seafloor massive sulfide (SMS) resources exceed 650 million metric tons [1]. In recent years, there has been increasing attention from countries worldwide towards these potential resources due to the development of green emerging technologies and the unique economic benefits associated with SMS deposits. Seafloor hydrothermal activities involve the exchange of materials and heat across multiple spheres, including the lithosphere, hydrosphere, and biosphere. These activities are accompanied by alteration of basement rocks and the precipitation of polymetallic sulfides and metalliferous sediments [2]. These products serve as evidence of seafloor hydrothermal circulation and provide a window to explore the formation and fluid evolution of seafloor hydrothermal systems

[3]. SMS deposits are products of submarine hydrothermal convection and are rich in metal elements such as Fe, Cu, Pb, Zn, Au and Ag. Due to their high ore grade, shallow occurrence depth, and rapid mineralization process, SMS deposits are deep-sea mineral resources with great economic potential [1,4]. Currently, the identification of SMS deposits mainly relies on detecting plumes, which are characterized by anomalies in water turbidity, temperature, and redox potential around hydrothermal fields (HFs), and then determining the hydrothermal vents [5,6]. However, for inactive sulfide deposits, electromagnetic and magnetic methods are considered effective approaches [7]. Nevertheless, sediment geochemistry exploration methods for SMS deposits offer potential but still need to be improved and supplemented [8].

Metalliferous sediments refer to polymetallic sulfides associated with submarine hydrothermal activities, as well as coexisting iron oxides, manganese oxides, and other components. Compared to pelagic sediments, they are enriched in Fe, Mn, Cu, Pb, Zn, and As but depleted in Al and Ti [9–14]. These submarine sediments adjacent to HFs are often influenced by hydrothermal activities, exhibiting mineralogical and chemical composition characteristics that are distinct from those of pelagic sediments [15]. Previous studies have identified two types of hydrothermal metalliferous sediments. The first type forms through the rapid deposition of sulfide material (metalliferous sediments near a vent), which can be considered cogenetic with massive sulfides and provides a record of hydrothermal ore-forming environments and processes [16]. The second type forms through particle settling from neutral-buoyancy hydrothermal plumes diluted by background sediments (metalliferous sediments far from a vent), this type is influenced by the hydrothermal plume dispersion patterns and processes [10,15,17], and is the proxy for the presence, intensity, and location of hydrothermal vents.

Significant progress has been made in the identification of metalliferous and nonmetalliferous sediments [18,19], the geochemical characteristics of hydrothermal metalliferous sediments [14,20–22], the ore-forming environment and genesis [23,24], and the history of hydrothermal sedimentation and evolution of hydrothermal activity [25–27]. However, there is still relatively limited research on the application of sediment geochemistry in hydrothermal exploration. Previous studies have characterized the distribution of hydrothermal-derived elements in surface sediments of the TAG HF on the Mid-Atlantic Ridge [28], the Dragon Horn HF in the Southwest Indian Ocean [8], and the Duanqiao-1 HF in the Southwest Indian Ocean [29], and have discussed the relationship between element distribution and distance from the vent. The published literature indicates that relevant work in various hydrothermal fields along the South Mid-Atlantic Ridge (SMAR) has not yet been conducted.

Since 2009, investigations and studies on hydrothermal activities on the SMAR have identified several hydrothermal fields, including Xunmei, Deyin, Tongguan, and Zouyu [30–35]. Recent research indicates that nonbiogenic sediments on the SMAR are primarily derived from hydrothermal sources, followed by rocks, with a small fraction precipitated from seawater [36]. However, there has been no relevant study on the genetic types and spatial distributions of hydrothermal components in surface sediments. In this study, surface sediments from 16 stations in the Xunmei HF were analysed using ICP-OES and ICP-MS for elemental geochemical analysis. By comparing the abundances of elements among these stations, we aim to understand the hydrothermal anomalies in the sediments and explore their relationship with hydrothermal vents and activities, thereby providing a geochemical basis for the identification of unknown hydrothermal vents.

The SMAR is divided into three secondary ridge segments (1N, 2N, and 3N) by the Rio Grande Transform Fault and the Moore Discontinuity Fault Zone [37]. The development of fault structures and volcanic activity provides conditions for hydrothermal circulation [38]. The Xunmei HF is located in the 2N ridge segment between 25°40′ and 26°35′ (Figure 1). It is approximately 100 km long and represents an asymmetric slow-spreading ridge, with a westward spreading rate of approximately 19.3 mm/yr and an eastward spreading rate of approximately 16.3 mm/yr [37,39]. In 2011, the Xunmei HF was discovered during the Chinese Ocean 22 expedition aboard the research vessel "Dayang

Preprints (www.preprints.org) | NOT PEER-REVIEWED | Posted: 15 August 2023 doi:10.20944/preprints202308.1072.v1

Yihao". In 2015, it was officially named the Xunmei HF by the China Ocean Mineral Resources Research and Development Association (COMRA).

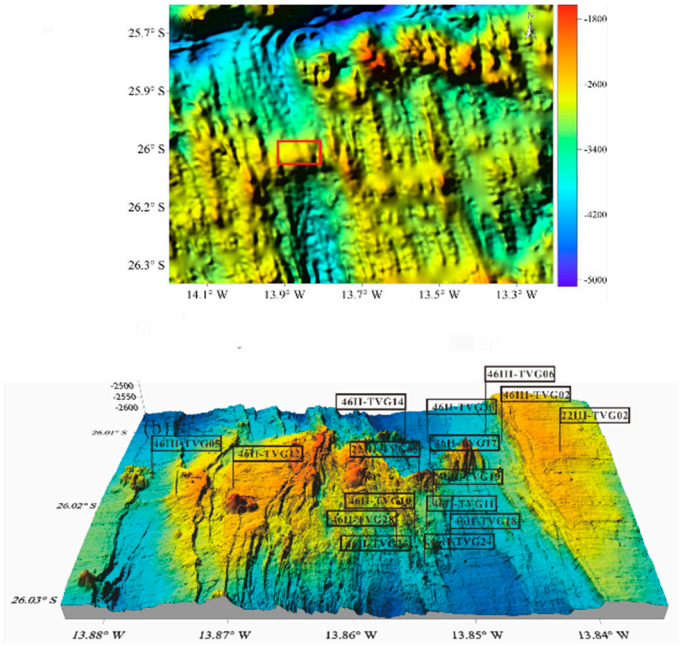

Figure 1. Location and topography of the Xunmei HF. The topographic data in (a) are from www.GEBCO.net, while the data in (b) are derived from AUV multibeam bathymetric surveys.

The HF is located in a depression between two volcanoes (Figure 1). At a water depth of approximately 2600 metres, a flat plateau has formed along a 7-9 kilometres wide axial valley [39]. The bedrock consists of N-MORB, with abundant occurrences of microcrystalline basalt, vesicular basalt, porous basalt, and basaltic glass [40,41]. The high-elevation fields are completely composed of pillow basalt, with a flat top and little sedimentation. In the low-elevation fields, fresh basalt is partially covered by loose sediment, and no ultramafic rocks are exposed [30]. Abundant metallic sulfide fragments, vent biota, chimney fragments, and inactive chimneys on slopes and low-lying fields were observed by camera tow surveys [2]. The detected temperature anomalies, presence of methane (CH_4), and widespread turbidity anomalies highlight the existence of hydrothermal vents in the Xunmei HF. A recent underwater video survey conducted in the Xunmei HF revealed the presence of three different types of sulfide chimneys. The iron-rich sulfide chimneys were predominantly composed of pyrite and marcasite, while the iron-copper-rich sulfide chimneys were mainly composed of pyrite and chalcopyrite. The copper-rich sulfide chimneys were primarily composed of chalcopyrite and pyrite [42]. In 2017, the Xunmei HF was reinvestigated during the Ocean Expedition 46. Although hydrothermal plumes were not observed at the survey site, many sulfide chimney samples were obtained using a TV grab sampler. These samples exhibited well-preserved internal structures with subtle surface changes, and showed abundant activity of tubeworms, indicating that the activity of these sulfide chimneys may have recently ceased.

2. Materials and Methods

Since 2009, the China Ocean Association has organized ocean expeditions to collect surface sediment samples at over 70 stations. The surface sediments used in this study were obtained from the segment III segment of the Ocean 22nd expedition and segments II and III of the Ocean 46th expedition using a TV grab sampler. A total of 16 surface sediment samples were collected within the depth range of 2445 to 2595 metres (Figure 1c and Table S1).

In addition, ten samples were collected at stations relatively far from the HF on the SMAR to represent the mineral compositions and elemental compositions of the background sediments (BGS). Among these samples, the closest distance to a known hydrothermal field is approximately 35 km,

Preprints (www.preprints.org) | NOT PEER-REVIEWED | Posted: 15 August 2023 doi:10.20944/preprints202308.1072.v1

while the other samples were from locations with distances ranging from 80 to 500 km from known vent sites. The characteristics of these sediments are light yellow to yellow calcareous mud containing foraminiferal shells, mixed with a certain amount of rock fragments. X-ray diffraction (XRD) analysis indicates that the sediments are mainly composed of calcite, with small amounts of goethite, hematite, and feldspar present in some samples.

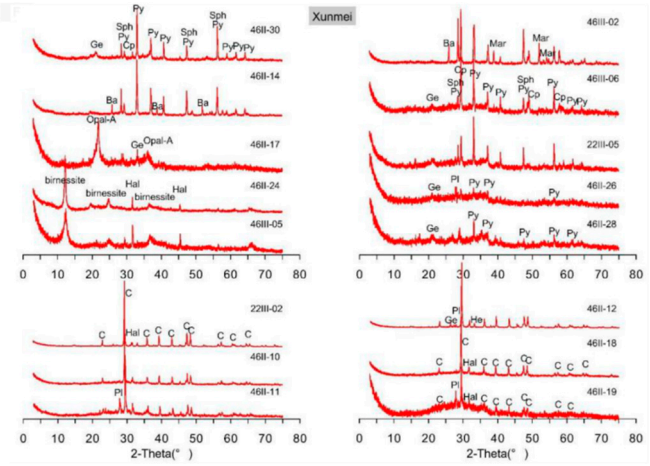

Figure 2. XRD analysis spectrum of surface sediments in the Xunmei HF[36].

Geochemical analysis was conducted at the Key Laboratory of Marine Geology and Metallogeny, the Ministry of Natural Resources. The pretreatment method for sediment samples was as follows: first, the powdered sample was dried in an 80°C oven. Then, precisely 50.00mg of the sample was weighed and placed in a digestion vessel, followed by the addition of 1.50mL of high-purity HNO_3 and 1.50mL of high-purity HF. The mixture was heated to 190°C for 48 hours to decompose. After cooling, it was evaporated to dryness. Then, 1.50mL of HNO_3 was added and evaporated to remove residual HF. Finally, the sample was heated to 150°C for 12 hours to dissolve. After cooling, the sample was prepared to a constant volume for analysis. The determination of major elements was conducted using ICP-OES, while trace and rare earth elements were measured using ICP-MS. Accuracy was controlled for both major and trace elements by analysis of reference solutions, namely Multielement Solution2 (CLMS-2), and the sulfide standard material (CRM) GBW07267, as well as blank and duplicate samples. The relative error was kept below 10%, and the relative standard deviation (RSD) was below 5%.

3. Results

The data for sediment major and trace elements are presented in Table 1. The complete geochemical analysis results can be found in Table S1.

Table 1. Major and trace elements of the sediments from Xunmei.

Elements	**Xunmei (n=16)**					**BGS (n=10)**	**Basalts (n=16)**	**Serpentinite (n=16)**
	Min	Max	Average	Median	SD	Average	Average	Average
Al(wt.%)	0.09	6.20	2.44	1.97	2.2	2.56	7.91	0.60
Si(wt.%)	2.78	19.54	11.32	11.64	5.38	6.31	23.75	18.40
Ca(wt.%)	0.23	26.55	7.37	3.30	8.74	28.84	8.58	0.37
Fe(wt.%)	4.58	38.78	21.25	20.49	12.36	2.24	6.84	6.05
K(wt.%)	0.10	0.75	0.22	0.14	0.19	0.28	0.09	-
Mg(wt.%)	0.16	4.04	1.82	1.58	1.24	1.58	4.84	22.42
Mn(wt.%)	0.04	24.29	2.91	0.34	7.03	0.12	0.13	0.09
Na(wt.%)	0.46	2.45	1.41	1.41	0.47	1.31	1.88	0.08

Preprints (www.preprints.org) | NOT PEER-REVIEWED | Posted: 15 August 2023 doi:10.20944/preprints202308.1072.v1

P(wt.%)	0.09	0.66	0.29	0.31	0.16	0.04	0.04	---
Ti(wt.%)	0.00	0.66	0.22	0.18	0.22	0.17	0.77	0.02
Ba(ppm)	31.04	1828	296.9	110.3	530.7	225.4	2.75	-
Sr(ppm)	11.30	1268	403.6	215.8	405.8	1251	112.6	
V(ppm)	73.94	806.1	330.7	317.3	190	63.45	266	38.91
Zn(ppm)	184	57,936	6922	3350	14263	40.87	71.59	36.28
Zr(ppm)	2.50	57.10	24.60	25.11	19.73	27.81	81.56	
Co(ppm)	16.63	304.6	114.9	91.65	72.82	23.00	40.93	89.65
Cu(ppm)	805.9	58286	16431	11514	16817	56.01	71.55	12.18
Ni(ppm)	2.87	335.4	51.85	35.81	78.55	53.12	71.46	1947
Cr(ppm)	16.37	232.5	101	88.01	68.42	65.18	324	1238
Sc(ppm)	0.54	33.84	11.91	11.00	11.18	8.58	40.43	
U(ppm)	0.33	11.48	4.15	3.66	3.36	0.42	0.05	
Y(ppm)	0.86	28.55	13.77	14.52	9.13	14.60	26.58	
Mo(ppm)	3.01	394.5	121.7	86.43	127.5	1.09	0.47	
Zr(ppm)	2.50	61.57	24.60	25.11	19.73	30.65	81.56	
MSI	0.32	42.08	14.26	10.30	14.33	44.09		
∑REE	1.64	51.66	28.30	32.61	17.29	50.24		
LREE	1.04	38.28	20.29	22.96	12.56	42.13		
HREE	0.60	15.36	8.01	9.24	5.23	8.1		
L/H	1.52	4.30	2.76	2.53	0.89	5.16		
δEu	0.88	4.53	1.58	1.04	1.11	0.84		
δCe	0.34	0.84	0.61	0.58	0.16	0.72		

3.1. Major elements

The Ca content of the sediments in Xunmei ranges from 0.23 to 26.55 wt.% (average = 7.37 wt.%), which is significantly lower than the Ca content of the background sediments (BGS: 28.84 wt.%, see Table 1). The contents of Al, Fe, and Mg range from 0.09 to 6.20 wt.%, 4.58 to 38.78 wt.%, and 0.16 to 4.04 wt.%, respectively, with average values of 2.44 wt.%, 21.25 wt.%, and 1.82 wt.%. The Fe content is significantly higher than that of the BGS, while the Al and Mg contents are relatively similar to those of the BGS. The Si and Ti contents are also relatively high, ranging from 2.78 to 19.54 wt.% and 0.00 to 0.66 wt.%, respectively. The average contents of K (0.22 wt.%), Mg (1.82 wt.%), and Na (1.41 wt.%) are similar to those of the BGS (0.28 wt.%, 1.58 wt.%, and 1.31 wt.% respectively). The average contents of Mn (2.91 wt.%) and P (0.29 wt.%) are one order of magnitude higher than those of the BGS (0.12 wt.% and 0.04 wt.% respectively).

3.2. Trace elements

The concentrations of Cu and Zn ranged from 805.87 to 58286 ppm and 184 to 57936 ppm, with average values of 16431 ppm and 6922 ppm, respectively. These concentrations were significantly higher than those of the BGS, but there were large differences in element concentrations among different samples. The Co concentration was relatively high (16.63 to 304.6 ppm, with an average of 114.9 ppm), which distinguishes it from other hydrothermal sediments in the field [8,12,29,43]. Heavy metals such as Cu, Zn, Fe, Mn, and Co in the Xunmei sediments were much higher than those in the BGS (Table 1). In addition, the average Cu/Al, Zn/Al, and Co/Al ratios in the Xunmei sediments (6734, 2837, and 47.09, respectively) were higher than the average values in the BGS (21.88, 15.96, and 8.98, respectively). The average concentrations of Ni and Cr were 51.85 ppm and 101 ppm, respectively; the Cr contents were slightly higher than those of the BGS (average of 65.18 ppm), while the Ni contents were similar to those of the BGS (average of 53.12 ppm). Notably, the sediments in Xunmei were significantly enriched in Mo (average of 121.7 ppm) and U (average of 4.15 ppm) compared to the BGS (average of 1.09 ppm for Mo and 0.42 ppm for U).

3.3. Rare earth elements

Preprints (www.preprints.org) | NOT PEER-REVIEWED | Posted: 15 August 2023 doi:10.20944/preprints202308.1072.v1

The total content of rare earth elements (∑REE) ranges from 1.64 to 51.66 ppm. The ratios of light rare earth elements to heavy rare earth elements (LREE/HREE) range from 1.52 to 4.30, indicating enrichment in LREEs (Figure 3a). All sediment samples show negative Ce anomalies (δCe ranges from 0.34 to 0.84, with an average of 0.61). Two types of Eu anomalies are observed in the sediment samples (Figure 3). Among them, samples 22III-TVG02, 46II-TVG10, 46II-TVG11, 46II-TVG12, and 46II-TVG28 exhibit slight negative Eu anomalies, while samples 46II-TVG14 and 46II-TVG24 show strong positive Eu anomalies (Table S1). The BGS-normalized REE patterns (Figure 3b) exhibit more pronounced positive Eu anomalies.

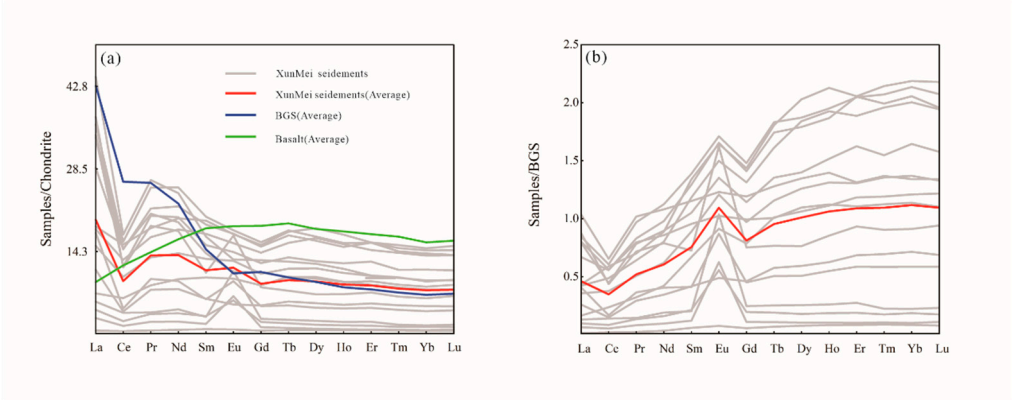

Figure 3. REE pattern normalization of sediments from Xunmei: (a) chondrite [44] and (b) background sediment (BGS). BGS: see Table S1; basalt: unpublished data.

4. Discussion

4.1. Sediment compositions

The sediments of the SMAR can be considered a mixture of background pelagic sediments (with constant Al/Mg ratios), basaltic or ultramafic debris (with low Al/Mg ratios), iron-manganese oxides, and hydrothermal components (without Al and Mg) [8].

Partial principal component analysis (PCA) of the major and trace elements in the Xunmei samples was performed using IBM SPSS Statistics 23 software. Based on the criterion of eigenvalues greater than 1 and after a varimax orthogonal rotation, a total of 4 principal factors were obtained (Table 2). The cumulative variance contribution rate of the 4 principal factors in the surface sediments of the Xunmei HF was close to 96%, therefore effectively representing the characteristics of all analysed samples. The specific analysis results are as follows: (1) The elements closely related to F1 are Al, Ti, Mg, Sc, and Y. Early studies have shown that Al and Ti may represent the detrital components of sediments[45], and they have high concentrations in the Xunmei samples (average content of Al is 2.44%, that of Ti is 0.22%). On the Al_2O_3-TiO_2 and Al_2O_3-MgO diagrams, both the BGS and the Xunmei sediments are mainly located within the linear range of basalt, indicating that their detrital components mainly come from basalt. Compared with the other stations, 46II-TVG14, 46II-TVG24, 46II-TVG30, and 46III-TVG05 contain more MgO, but the content is lower than that of serpentinite. Regardless of the tectonic background, the content of Mg in hydrothermal fluids is less than 1 ppm [46]. The higher MgO contents in the sediments of the Dragon Horn, Saladaha, and Rainbow HFs is due to the presence of a large amount of ultramafic debris [8,26,43], but the basement rocks in the Xunmei field are N-MORB [40], and no ultramafic rocks are exposed. Therefore, the enrichment of MgO cannot originate from the input of ultrabasic rock fragments. Considering that the four stations are located on the edge of the hydrothermal field with lower terrain, the enrichment of MgO may also be contributed by the weathering products of basalt at higher elevations. (2) The elements closely associated with the F2 factor include Mn, Mo, K, and Ba, representing elements scavenged from seawater during the migration process of neutral-buoyancy hydrothermal plumes. (3) In the F3 factor, Fe, Cu, and U are positive loadings, representing Fe oxyhydroxides, hydrothermal Cu, and other nonbuoyant hydrothermal plume particles, while Ca is a negative loading,

Preprints (www.preprints.org) | NOT PEER-REVIEWED | Posted: 15 August 2023 doi:10.20944/preprints202308.1072.v1

representing calcium biogenic components. (4) The F4 factor is closely related to Zn and Cu and is primarily associated with sulfides, representing the contribution of sulfide chimney fragments.

Table 2. Results of factor analysis of surface sediments.

	F1	F2	F3	F4
Eigenvalue	7.306	3.615	1.427	1.008
Cumulative%	52.183	78.003	88.196	95.397
Al	0.925	-0.320	-0.160	-0.113
Fe	-0.427	-0.182	0.757	0.354
Mn	-0.110	0.977	-0.062	-0.055
Zn	-0.301	-0.067	0.064	0.935
Cu	-0.119	-0.262	0.566	0.698
Mo	-0.356	0.794	0.420	0.088
U	-0.375	-0.047	0.884	-0.129
Ti	0.925	-0.303	-0.194	-0.091
Mg	0.958	0.002	-0.203	-0.162
K	-0.249	0.926	0.084	-0.148
Sc	0.919	-0.284	-0.236	-0.116
Y	0.794	-0.216	-0.397	-0.309
Ba	-0.176	0.943	-0.146	-0.082
Ca	0.144	-0.331	-0.841	-0.301

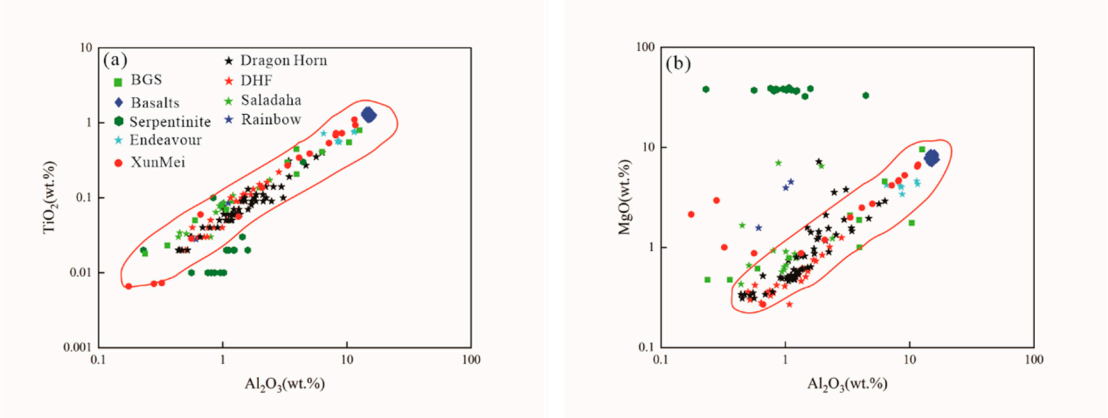

Figure 4. Al_2O_3-TiO_2 (a) and Al_2O_3-MgO (b) diagrams. Data sources: Endeavour: [12]; Dragon Horn: [8]; DHF: [29]; Saladaha and Rainbow: [43]; Serpentinite: [47]; Basalt: unpublished data.

Yang et al. [36] utilized geochemical quantification criteria, namely, an Fe content (carbonate-free basis) >10% (without carbonate substrate) and an Al/(|Al+Fe+Mn|) value of <0.4, to differentiate between metalliferous and nonmetalliferous sediments. Among them, 15 samples were classified as metalliferous sediments. The metalliferous sediment index (MSI=100*Al/(|Al+Fe+Mn|)) of the sediments ranged from a maximum of 42.08% to a minimum of 0.32%, indicating significant metal enrichment in the sediments (see Table S1).

On the Fe-Al-Mg diagram, the BGS are similar to the basaltic rocks (Figure 5a). However, unlike the basaltic rocks, the BGS exhibit higher manganese contents and similar iron contents (Figure 5b). Considering that the BGS sampling locations are far from known hydrothermal fields, it is unlikely that the iron and manganese originate from hydrothermal sulfides, indicating the presence of significant amounts of iron oxyhydroxides and manganese oxides. The Xunmei sediments are enriched in Cu, Zn, and Fe (Figures 5a, b, c), suggesting the input of hydrothermal-derived components. The high concentrations of Cu, Zn, and Fe in the Xunmei HF compared to other regions are believed to be from sulfides [28]. The Xunmei sediments exhibit a Cu-Zn enrichment pattern, different from the Fe-Cu enrichment pattern observed in the DHF, Dragon Horn, and Endeavour HFs

Preprints (www.preprints.org) | NOT PEER-REVIEWED | Posted: 15 August 2023 doi:10.20944/preprints202308.1072.v1

(Figure 5c). Additionally, the Xunmei sediments have lower MSI values. These characteristics indicate a higher abundance of hydrothermal components in the sediments.

On the Si-Fe-10Mn diagram, the majority of the samples of Xunmei sediments are located closer than basalt, the BGS and other hydrothermal sediments to the iron endmember. Only stations 46II-TVG24 and 46III-TVG05 are located closer to manganese, indicating that the main component of the majority of the samples is iron oxyhydroxide, while the sediments at stations 46II-TVG24 and 46III-TVG05 are mainly composed of manganese oxides.

Previous studies have shown that hydrothermal fluids in mid-ocean ridges are typically enriched in LREEs, exhibit significant positive Eu anomalies, and lack Ce anomalies [48]. However, sediment samples from the Xunmei display two distinct patterns of REEs (Figure 3): one with a clear positive Eu anomaly, similar to the hydrothermal fluid REE pattern; and another with no Eu anomaly and no negative Ce anomaly. This is interpreted as the occurrence of phase separation in the hydrothermal fluids, resulting in two distinct patterns of REEs (positive Eu anomalies and no anomalies), and the precipitation of sulfides and sediments similar to the hydrothermal fluids [36].

The comparative diagram of Fe/Ti and Al/(Al+Fe+Mn) (Figure 6) illustrates the relative contributions of hydrothermal and detrital components in the surface sediments. The decrease in Fe/Ti ratios and the increase in Al/(|Al+Fe+Mn|) ratios indicate the dilution of metalliferous sediments by pelagic sediments [43]. The sediment compositions in Xunmei fall between the BGS and the metalliferous sediments. In conclusion, the sediments in Xunmei can be interpreted as a mixture of BGS, basaltic debris, iron-manganese oxides, and hydrothermal components.

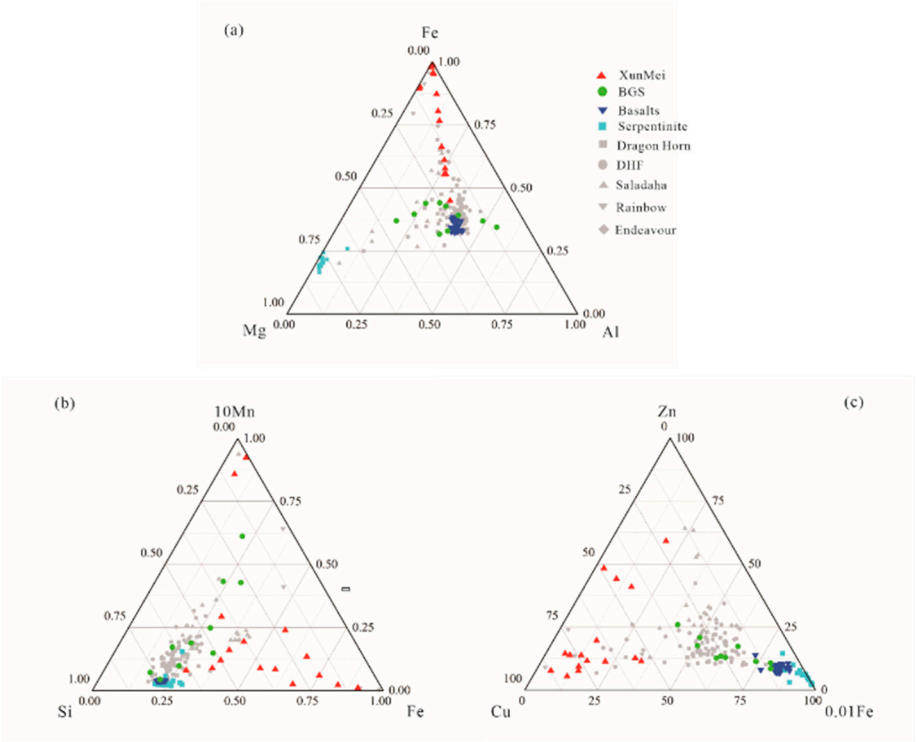

Figure 5. Fe-Al-Mg(a), Si-Fe-10Mn(b) and Cu-0.01Fe-Zn(c) diagrams of sediment compositions.Data source: Same as Figure 4

Preprints (www.preprints.org) | NOT PEER-REVIEWED | Posted: 15 August 2023 doi:10.20944/preprints202308.1072.v1

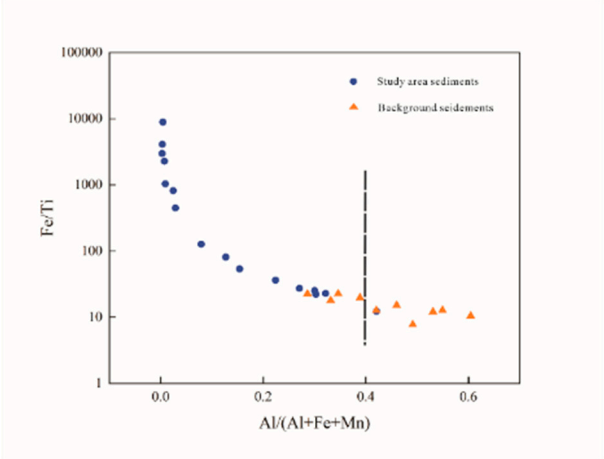

Figure 6. Al/(Al+Fe+Mn) vs. Fe/Ti diagram.

4.2. Distribution characteristics of hydrothermal-derived elements in sediments

According to the methods proposed by references [8,26], the contribution of each endmember to the compositions of sediments can be calculated using the following procedure:

The elemental content of surface sediments can be directly obtained through analysis. Since the exposed wallrock in Xunmei is predominantly basalt [40], which has a significantly higher Al_2O_3 content than ultramafic rocks (Table 1), it can be assumed that the Al in the sediments of Xunmei mainly originates from basaltic debris. Therefore, the content of elements derived from basaltic debris can be calculated using the following formula:

$$Element_{Basaltic} = (Element/Al)_{background} * Al_{total}.$$

$Element_{Basaltic}$: elements derived from basaltic debris; $(Element/Al)_{background}$: the ratios of other elements in the background sediments to Al; and Al_{total}: the content of Al in Xunmei sediments.

The iron-manganese oxides in the sediments of mid-ocean ridges are typically the precipitates of neutral-buoyancy hydrothermal plumes [29]. Therefore, it can be assumed that the residual element abundance, after subtracting the contribution from debris, represents the hydrothermal contribution. The calculation formula is as follows:

$$Element_{Hydrothermal} = Element_{Total} - Element_{Basaltic}.$$

$Element_{Hydrothermal}$: elements derived from hydrothermal processes and their related elements. $Element_{Total}$: the content of specific elements in the Xunmei sediments. $Element_{Basaltic}$: elements derived from basaltic debris.

4.2.1. Cu, Zn, Fe, Co

Previous studies have shown that elements in hydrothermal plumes exhibit three main behaviours compared to the dominant element Fe: (1) elements with a preference for Cu and other sulfide precipitates are rapidly lost from the hydrothermal plume due to preferential settling or oxidative dissolution; (2) elements primarily present in seawater as oxyanions appear to coprecipitate with iron oxyhydroxides in the early stages of hydrothermal plume formation, exhibiting a constant ratios with iron; and (3) particle-reactive elements such as Be, Y, Th, and REEs show an increasing elemental ratios with Fe, indicating continuous scavenging from seawater onto precipitated oxyhydroxide particles [49–51].

In the sediments of the Xunmei HF, Fe exhibits higher concentrations in the southern and northern regions, while lower concentrations are observed in the central depression. Copper and iron show similar distribution patterns (Figure 7a, c). The higher concentrations in the southern and northern regions indicate that the surface sediments in this field have received more input of hydrothermal Cu and Fe. Additionally, the higher maturity of chimneys in the southern region and the entry of altered secondary minerals into the sediments may also contribute to the enrichment of Cu and Fe. In contrast, Zn shows a different distribution pattern, with the highest concentrations in

Preprints (www.preprints.org) | NOT PEER-REVIEWED | Posted: 15 August 2023 doi:10.20944/preprints202308.1072.v1

the northeast and much lower concentrations in other regions (Figure 7b). The highest concentrations of Cu and Zn are both found in the northeast at station 46III-TVG02. In comparison, Fe exhibits four high concentration centres (46II-TVG14, 46II-TVG28, 46II-TVG30, 46III-TVG02), with the highest values occurring in the northern region (46II-TVG14 and 46II-TVG30). Previous studies have shown that Cu, Zn, and Fe are significantly enriched at the source, but compared to Fe, the concentrations of Cu and Zn decrease more rapidly with increasing distance from the vent and are predominantly deposited as sulfides [12,26,29]. In contrast to Cu and Fe, the distribution of Co is relatively uniform, with the highest value occurring in the northern region at station 46II-TVG14 (Figure 7d). In the Duanqiao-1 HF, Co exhibits two peaks in its lateral distribution, which are interpreted as the early incorporation of Co into the structure of sulfides during the formation of hydrothermal plumes, and the second enrichment is due to the continuous mixing of hydrothermal plumes with seawater, resulting in the scavenging of Co from seawater onto oxides [29]. In the Xunmei HF, Co does not show any significant correlation with other elements, suggesting that Co may be enriched from two sources: sedimentation from hydrothermal plumes and input of chimney debris.

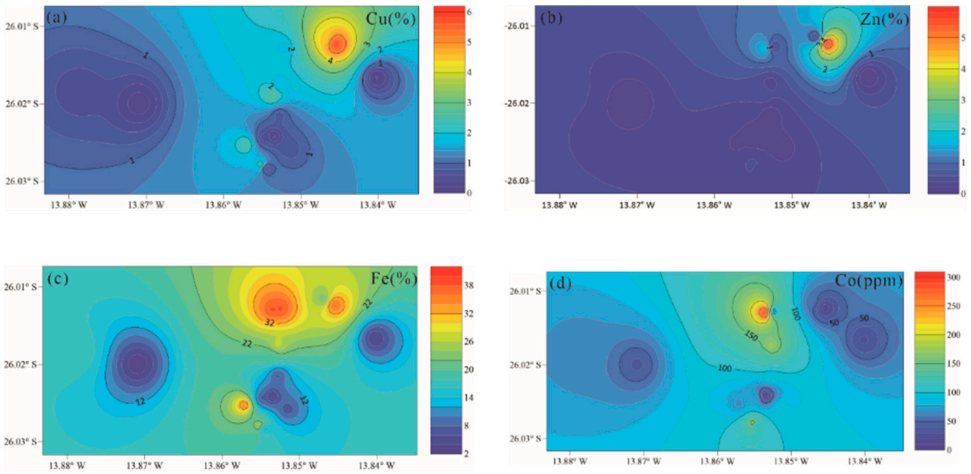

Figure 7. The distributions of Cu, Zn, Fe, Co.

4.2.2. Mn, V, Mo, U, P

The distribution characteristics of Mn are unique. The highest value of Mn is found in the western region at station 46III-TVG05, while the second highest value is found in the southern region at station 46II-TVG24 (Figure 8a). The central region has the lowest content, with some stations even showing negative values (46III-TVG06, 46II-TVG11), indicating no Mn input associated with hydrothermal activity. There is no clear correlation between Fe and Mn, suggesting that these two metals and their associated elements exist in different stages of sedimentation [28]. Compared to Fe, Mn precipitates relatively slowly; therefore, Mn tends to be slowly removed from hydrothermal plumes in dissolved form and deposited into sediments throughout the suspension and neutral-buoyancy plumes [52,53]. Under reducing conditions, the migration distance of Mn increases. For example, in the Dragon Horn field, Mn precipitates at distances greater than 60 km [8]. The high anomalous values of Mn in sediments from the western station 46III-TVG05 and the southern station 46II-TVG24 suggest the presence of relatively oxidized environments near the Xunmei HF.

The distribution of P is similar to that of Cu and Fe, with higher concentrations in the northern and southern parts and the lowest concentration in the central part. The highest value of P is found in the southern part at station 46II-TVG26 (Figure 8e). The highest value of V coincides with that of Mn (Figure 8b), but at station 46II-TVG24, V has the lowest value, while Mn has the second highest value. According to traditional views, V is usually derived from seawater and coprecipitates with oxyhydroxides [51]. It is believed that the P/Fe ratios and V/Fe ratios do not change after the formation of neutral-buoyancy plumes [49,54]. However, in the Rainbow HF, the P/Fe ratios reported by Edmonds and German [51] remain consistent throughout the hydrothermal plume, matching the P/Fe ratios in the hydrothermal component of the surface sediments. On the other hand, the V/Fe

Preprints (www.preprints.org) | NOT PEER-REVIEWED | Posted: 15 August 2023 doi:10.20944/preprints202308.1072.v1

ratios gradually increase from the early plume to the sediment. This is consistent with the strong positive correlation observed between P and Fe in Xunmei (R=0.782, P=0.000, N=16), indicating that P from seawater coprecipitates with Fe from the hydrothermal plume. The V/Fe ratios in the sediment show significant variability, and V is not significantly correlated with Fe. The anomalous portion of V is mainly derived from sulfides, which have low V/Fe ratios and dilute the primary signal derived from the hydrothermal plume [55].

The high-value fields of Mo are mainly found in the western and southern Xunmei (Figure 8c), and they overlap with those of Mn, with Mo showing a strong positive correlation with Mn (R=0.781, P=0.000, N=16). Previous studies have suggested that Mo is coprecipitates with iron sulfides when reduced to Mo(IV), while Mo(V) and V(IV) are scavenged by the surface of oxidized phases in sediments [56]. Therefore, Mo in the Xunmei field is primarily scavenged and coprecipitated with manganese oxides in the form of Mo(V). The distribution pattern of U is similar to that of P, and U shows a strong positive correlation with both P and Fe (U and P, R=0.764, P=0.001, N=16; U and Fe, R=0.760, P=0.001, N=16). It is generally believed that the main source of U in marine metalliferous sediments is seawater and to a lesser extent with detrital components (with possible mantle contributions) [12,57,58]. Mills et al. [57] showed that the enrichment of U in iron-capped sediments in the TAG field of the Mid-Atlantic Ridge can be attributed to seawater diffusion into sulfide-derived sediments. In addition to seawater, U in metalliferous sediments has detrital sources and is associated with clay fractions, phosphates, and organic matter in sediments [58,59]. As shown in Table 1, the U contents in basalt and the BGS are low (average values of 0.05 ppm and 0.42 ppm, respectively), which does not support a detrital source for this element. Furthermore, the high concentrations of U, Th, Au, Hg, and ^{3}He, provide evidence for a mantle source of these elements. Apart from U, the remaining elements are not significantly enriched in Xunmei, and some are even below the detection limit, thus ruling out a mantle source. Considering the strong positive correlations between U and P and Fe, the most likely source of the U is seawater via coprecipitation with hydrothermal Fe.

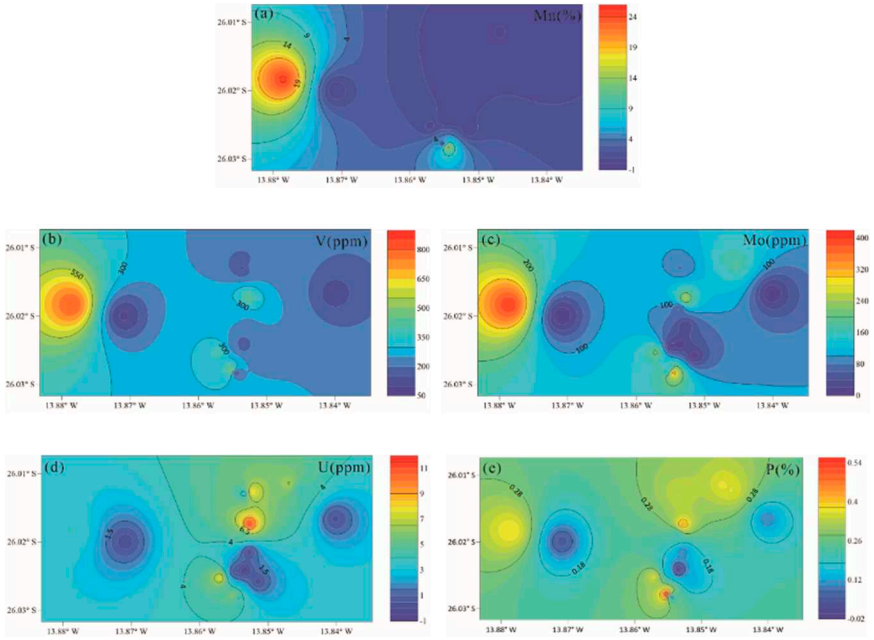

Figure 8. The distributions of Mn, V, Mo, U, P.

4.3. Geochemical characteristics of different regional hydrothermal activities

In Xunmei, 16 sediment samples were obtained, all of which, except for station 46II-TVG11, were metalliferous sediments (see Table S1). Although the measured MSI can serve as a useful tracer to indicate the presence of hydrothermal input in deep-sea sediments, it may not provide any sensitive indication of the distance between the sediment and the hydrothermal source [21]. To discern more "directional" information, different chemical indicators must be utilized.

 doi:10.20944/preprints202308.1072.v1

Numerous studies have shown that Cu and Zn are significantly enriched at the vent, primarily distributed in the form of sulfides within a limited distance from the hydrothermal field, and their concentrations decrease significantly with increasing distance from the vent. This has been confirmed in multiple hydrothermal fields [8,12,26]. However, there is no consensus on the deposition sequence of different elements, with the focus mainly on the precipitation sequence of Cu and Zn. Mottl and Mcconachy [52] determined that the enrichment of elements in hydrothermal plumes follows the sequence of Cu, Co, Cd, Zn, Pb, and Ni, while Cave et al. [26] found that, compared to Cu and Fe in the Rainbow HF, Zn preferentially precipitates in the form of sulfides near the vent, Edmonds and German [51] found that chalcophile elements are preferentially removed from hydrothermal fluids in the order of Cd, Zn, Co, and Cu. In the Dragon Horn field, the spatial distribution of hydrothermal Zn is significantly limited compared to that of Cu, occurring only within a range of ≤3 km from the hydrothermal vent, indicating that Zn precipitates earlier than Cu from the hydrothermal plume. The Cu/Fe ratios in the Duanqiao-1 HF decrease slightly faster than the Zn/Fe ratios relative to the background value, suggesting that Cu precipitates earlier than Zn [8,29].

The Cu/Fe ratios of the sediments in the Xunmei HF range from 0.012 to 0.195 (Figure 9a), while the Zn/Fe ratios range between 0.005 and 0.158 (Figure 9b). Compared to those of the BGS, the Cu/Fe ratios in the Xunmei sediments are higher by one to two orders of magnitude. The values at stations 22III-TVG05, 46III-TVG06, and 46III-TVG02 are significantly higher than those at the other stations. These findings suggest that as the distance from the vent increases, the Cu/Fe ratios in the sediments decrease significantly. This fractionation is attributed to the preferential settling of sulfide material over low-density oxide material in dispersed neutral-buoyancy plumes [60]. Prior to the discovery of the TAG HF, active vents were believed to be located near the eastern wall of the MAR rift at 26°N. Shearme et al. [28] analysed the core-top geochemical samples that exhibited the highest Cu/Fe ratios and clearly delineated the location of the subsequently discovered TAG hydrothermal mound [61]. Additionally, Cave et al. [26] confirmed a systematic decrease in Cu/Fe ratios in core-top samples at locations far from the Rainbow HF. Apart from the significantly elevated ratios at station 46III-TVG02, the differences in the Zn/Fe ratios relative to the BGS were smaller than those in the Cu/Fe ratios. This is attributed to the widespread occurrence of Fe sulfides and Cu-Fe sulfides in the Xunmei HF, where the Zn sulfide content is low and distributed sporadically, as Zn is naturally less abundant in hydrothermal fluids.

The dispersion distance of Fe and Mn is much greater than that of Cu and Zn, as previous studies have shown that Fe and Mn in hydrothermal plumes can migrate over long distances and deposit outside the hydrothermal field in the form of iron and manganese-rich sediments [62], indicating that Fe and Mn can be transported to locations far from the hydrothermal field. Liao et al. [29] found that Fe precipitates in the range of 60 km from the hydrothermal field in the Duanqiao-1 HF, while Mn can disperse to locations beyond 60 km from the field, suggesting that Fe precipitates faster than Mn. The oxidation rate of Mn in seawater is slower than that of Fe; therefore, it is expected that the Mn/Fe ratios of particles deposited by hydrothermal plumes will increase with increasing distance from the source [63]. The Fe/Mn ratios in the Xunmei HF range from 0.69 to 1440 (Figure 9c). The Fe/Mn ratios exhibit significant variations, with three sample stations below the background value and six stations (22III-TVG05, 46II-TVG14, 46II-TVG19, 46II-TVG30, 46III-TVG02, 46III-TVG06) significantly higher than the background value. The remaining stations show ratios similar to the background value. The highest ratio is observed at the northeastern station 46III-TVG02, reaching a value of 1440. This station is located within the vicinity of metalliferous sediments near the vent in the Lucky Strike HF (1000-3000), TAG HF (900-2000), OBS HF (900-2400), and Wocan-1 HF (1373-1475). Therefore, it can be inferred that this station is likely a proximal to the vent [53,64–66].

Preprints (www.preprints.org) | NOT PEER-REVIEWED | Posted: 15 August 2023 doi:10.20944/preprints202308.1072.v1

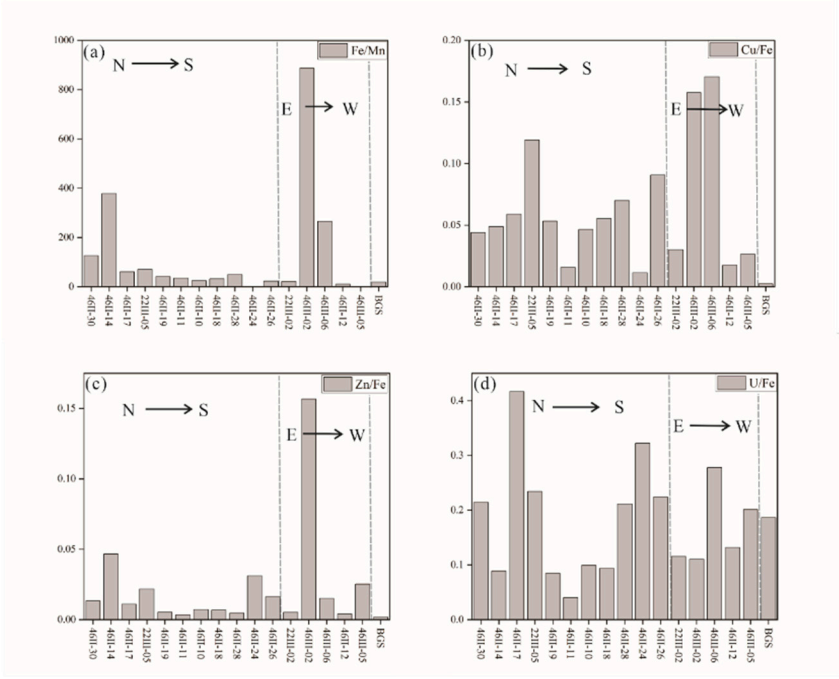

Figure 9. Ratios of Cu/Fe (a), Zn/Fe (b), Fe/Mn (c), and U/Fe (d) in sediment derived from hydrothermal activity at different sampling sites. Note: Background values were used for sites without hydrothermal input. N-North, S-South, E-East, W-West.

In summary, to determine the relative positions of sediment and vents, it is necessary to first consider the contents of Cu and Zn. Cu and Zn tend to precipitate near the vent and rapidly decrease with increasing distance from the vent, which effectively indicates the location of the vent [8,17,51,64]. In addition, the ratios of Cu/Fe, Zn/Fe, and Fe/Mn can also determine the distance relationship between sediments and vents. This is because the ratios of Cu/Fe, Zn/Fe, and Fe/Mn in sediments near the vents are higher, and in the TAG and OBS HFs, these ratios effectively determine the proximal source of the sediments [53].

Based on the variations in Cu and Zn contents, multiple indicators such as Cu/Fe, Zn/Fe, and Fe/Mn ratios (Figure 7a, b and Figure 9a, b, c), were used to determine the presence of high-temperature hydrothermal vents near station 46III-TVG02 in the northeastern Xunmei. Previous studies have indicated secondary oxidation of sulfides in hydrothermal environments by the increase in U/Fe ratios in metal deposits [11,57,64–66]. Additionally, the high concentration of U in hydrothermal sediments is consistent with scavenging from seawater and sulfide oxidation [11,64,65]. The combined U/Fe ratios (Figure 9d) and the topography of Xunmei indicate that stations located at lower elevations have higher U/Fe ratios than the background values. Conversely, stations at higher elevations have lower ratios compared to the background values, suggesting higher oxidation rates of sulfides at lower elevations. The U/Fe ratio at station 46III-TVG02 is lower than the background value, indicating that sulfides at this location have not undergone secondary oxidation and have a lower maturity level.

The combination of the distribution characteristics of metal elements such as Cu, Fe, and Co (Figures 7a, c, d) and elements such as U and P (Figures 8d, e) that are highly correlated with Fe reveals that in addition to the northern part of Xunmei, the southern part also features high values of the corresponding elements, indicating the possible presence of hydrothermal vents in southern Xunmei. The distribution range of elements in the southern part is narrower than that in the northern part, indicating that the eruption time of the vents in the southern part was shorter than that in the northern part. Furthermore, investigations have revealed that the chimneys in southern Xunmei have a higher maturity and greater alteration compared to those in the northern part, suggesting that the vents in this area may have been inactive for a long time.

In the Xunmei HF, the western station 46III-TVG05 and southern station 46II-TVG24 exhibit Mn anomalies that are one to two orders of magnitude higher than those of other stations. The concentrations of Cu and other metal elements at these two stations are relatively low, indicating that the high Mn contents cannot be attributed to the collapse of hydrothermal sulfide chimneys. As mentioned earlier, Mn can migrate outside the hydrothermal field, and under reducing conditions, the migration distance can be greater. From the similar distribution patterns of Mn, V, and Mo (Figure 8a, b, c), it can be inferred that there is a relatively oxidizing environment at the edge of the Xunmei field, which is consistent with the high U/Fe ratios in this region.

In summary, there are high-temperature hydrothermal vents located in the northeastern part of the Xunmei HF, while in the southern region, there are inactive vents with a shorter eruptive duration. At the edges, a relatively oxidized environment is present.

5. Conclusion

The sediment in Xunmei is predominantly composed of metalliferous sediments, which are a mixture of background sediments, basalt debris, iron-manganese oxides, and hydrothermal components. These sediments are significantly enriched in Cu, Zn, Fe, Co, as well as elements primarily scavenged from seawater such as Mn, V, Mo, U, and P.

The spatial distribution of hydrothermal elements in sediments exhibits significant variations. The highest concentrations of Cu and Zn are found in the northeastern part of Xunmei, and Fe shows three high-concentration regions in the northeastern, northern, and southern parts of Xunmei. Manganese exhibits abnormally high concentrations in the western and southern parts of Xunmei. U and P primarily coprecipitate with Fe in hydrothermal plumes, and Mo is mainly scavenged by manganese oxides. Vanadium is primarily scavenged by hydrothermal plumes and precipitates to the sediments, and Co primarily originates from the collapse of sulfide chimneys.

Based on the variations in Cu and Zn concentrations, as well as the Cu/Fe, Zn/Fe, and Fe/Mn ratios, high-temperature hydrothermal vents were inferred to exist near station 46III-TVG02. The distribution patterns of Cu, Fe, Co, and other elements suggest the possible presence of hydrothermal vents in southern Xunmei. The anomalously high values of Mn and the high U/Fe ratios suggest the possible existence of relatively oxidized environments in Southern Xunmei.

Future geochemical investigations on sediment core samples are essential to have a better understanding of the evolution of the hydrothermal process in the Xunmei HF.

Supplementary Materials: Table S1: Major and trace element compositions of the bulk sediment of the Xunmei hydrothermal field. Table S2: Partial principal component analysis (PCA) of the major and trace elements in the sediment samples from Xunmei. Table S3: Correlation analysis of hydrothermal-derived elements of the sediments in the Xunmei field.

Author Contributions: L.C. collected the samples and conceived designed and fund the study; Y.P. wrote the first draft (with contributions from all other co-authors); Y.B. analyzed the major and trace elements of bulk samples; F.L. and D.D. co-supervised the project; G.Y. supplied the data of basalts; Z.Q. designed the bathymetric map; D.Y co-supervised the project and fund the study.

Funding: This study was financially supported by Basic Scientific Fund for National Public Research Institutes of China (No.2021Q01), National Natural Science Foundation of China (No.42006180), and China Ocean Mineral Resources R&D Association (No. DY135-S2-2).

Acknowledgments: The authors sincerely appreciate the captains and crew of R/V Dayangyihao (DY 22th) and R/V Xiangyanghong01 (DY46th) for their immense support during the investigations and sampling of the Xunmei hydrothermal field.

Conflicts of Interest: : The authors declare no conflict of interest.

References

1. Hannington, M.; Jamieson, J.; Monecke, T.; Petersen, S.; Beaulieu, S., The abundance of seafloor massive sulfide deposits. *Geology* **2011,** *39* (12), 1155-1158.

2. Li, T.; Yang, Y.; Wang, G.; Fan, L.; Wang, C.; Li, B., The Mineralogical Characteristics of Pyrite at 26°S Hydrothermal Field, South Mid-Atlantic Ridge. *Acta Geologica Sinica - English Edition* **2014,** *88* (s2), 179-180.
3. Zhu, Q.; Zhou, H., Research status and prospects of metalliferous sediments in hydrothermal vents. *Marine Science* **2021,** *45* (08), 69-80.
4. Luo, H.; Han, X.; Wang, Y.; Wu, X.; Cai, Y.; Yang, M., Exploring the Mechanism and Resource Prospects of Strategic Metal Enrichment in Global Modern Seafloor Massive Sulfides. *Earth Science-Journal of China University of Geosciences* **2021,** *46* (9).
5. Tao, C.; Li, H.; Yang, Y.; Ni, J.; Cui, R.; Chen, Y.; Li, J.; He, Y.; Huang, W.; Lei, J.; Wang, Y., Two hydrothermal fields found on the Southern Mid-Atlantic Ridge. *Science China Earth Sciences* **2011,** *54* (9), 1302-1303.
6. Tao, C.; Li, H.; Jin, X.; Zhou, J.; Wu, T.; He, Y.; Deng, X.; Gu, C.; Zhang, G.; Liu, W., Seafloor hydrothermal activity and polymetallic sulfide exploration on the southwest Indian ridge. *Chinese Science Bulletin* **2014,** *59* (19), 2266-2276.
7. Chen, S.; Tao, C.; Zhou, J.; Zhang, G.; Qin, H.; Wang, Y.; Chen, D., Distribution characteristics of hydrothermal plumes on the mid-ocean ridge and their indicative role in polymetallic sulfide exploration. *Acta Oceanologica Sinica* **2019,** *41* (08), 1-12.
8. Liao, S.; Tao, C.; Li, H.; Zhang, G.; Liang, J.; Yang, W.; Wang, Y., Surface sediment geochemistry and hydrothermal activity indicators in the Dragon Horn area on the Southwest Indian Ridge. *Marine Geology* **2018,** *398*, 22-34.
9. Dymond, J.; Corliss, J. B.; Heath, G. R.; Field, C. W.; Dasch, E. J.; Veeh, H. H., Origin of Metalliferous Sediments from the Pacific Ocean. *Geological Society of America Bulletin* **1973,** *84* (10), 3355-3372.
10. Mills, R.; Elderfield, H.; Thomson, J., A dual origin for the hydrothermal component in a metalliferous sediment core from the Mid-Atlantic Ridge. *Journal of Geophysical Research* **1993,** *98* (B6).
11. Gurvich, Metalliferous sediments of the world ocean: fundamental theory of deep sea hydrothermal sedimentation. **2006**.
12. Hrischeva, E.; Scott, S. D., Geochemistry and morphology of metalliferous sediments and oxyhydroxides from the Endeavour segment, Juan de Fuca Ridge. *Geochimica et Cosmochimica Acta* **2007,** *71* (14), 3476-3497.
13. Bodeï, S.; Buatier, M.; Steinmann, M.; Adatte, T.; Wheat, C. G., Characterization of metalliferous sediment from a low-temperature hydrothermal environment on the Eastern Flank of the East Pacific Rise. *Marine Geology* **2008,** *250* (1-2), 128-141.
14. Dekov, V. M.; Cuadros, J.; Kamenov, G. D.; Weiss, D.; Arnold, T.; Basak, C.; Rochette, P., Metalliferous sediments from the H.M.S. Challenger voyage (1872–1876). *Geochimica et Cosmochimica Acta* **2010,** *74* (17), 5019-5038.
15. Feely, R. A.; Lewison, M.; Massoth, G. J.; Robert-Baldo, G.; Lavelle, J. W.; Byrne, R. H.; Von Damm, K. L.; Curl, H. C., Composition and dissolution of black smoker particulates from active vents on the Juan de Fuca Ridge. *Journal of Geophysical Research: Solid Earth* **1987,** *92* (B11), 11347-11363.
16. Blanc, G.; Anschutz, P.; Pierret, M.-C., Metalliferous sedimentation in the Atlantis II Deep: a geochemical insight. In *Sedimentation and Tectonics in Rift Basins Red Sea:- Gulf of Aden*, Purser, B. H.; Bosence, D. W. J., Eds. Springer Netherlands: Dordrecht, 1998; pp 505-520.
17. Feely, R. A.; Massoth, G. J.; Baker, E. T.; Lebon, G. T.; Geiselman, T. L., Tracking the dispersal of hydrothermal plumes from the Juan de Fuca Ridge using suspended matter compositions. *Journal of Geophysical Research: Solid Earth* **1992,** *97* (B3), 3457-3468.
18. Boström, K.; Kraemer, T.; Gartner, S., Provenance and accumulation rates of opaline silica, Al, Ti, Fe, Mn, Cu, Ni and Co in Pacific pelagic sediments. *Chemical Geology* **1973,** *11* (2), 123-148.
19. Boström, K.; Peterson, M. N. A.; Joensuu, O.; Fisher, D. E., Aluminum-poor ferromanganoan sediments on active oceanic ridges. *Journal of Geophysical Research* **1969,** *74* (12), 3261-3270.
20. Barrett, T. J.; Jarvis, I.; Hannington, M. D.; Thirlwall, M. F., Chemical characteristics of modern deep-sea metalliferous sediments in closed versus open basins, with emphasis on rare-earth elements and Nd isotopes. *Earth-Science Reviews* **2021,** *222*.
21. German, C. R., Hydrothermal activity on the eastern SWIR (50°-70°E): Evidence from core-top geochemistry, 1887 and 1998. *Geochemistry, Geophysics, Geosystems* **2003,** *4* (7).
22. Yu, Z.; Li, H.; Li, M.; Zhai, S., Hydrothermal signature in the axial-sediments from the Carlsberg Ridge in the northwest Indian Ocean. *Journal of Marine Systems* **2018,** *180*, 173-181.
23. Yang, B.; Liu, J.; Shi, X.; Zhang, H.; Wang, X.; Wu, Y.; Fang, X., Mineralogy and sulfur isotope characteristics of metalliferous sediments from the Tangyin hydrothermal field in the southern Okinawa Trough. *Ore Geology Reviews* **2020,** *120*.
24. Yang, B.; Wu, Y.; Wang, X.; Zhang, Y.; Cui, J.; Yu, M.; Dang, Y.; Shi, X.; Liu, J., Mineralogical and geochemical characteristics and ore-forming mechanism of hydrothermal sediments in the middle and southern Okinawa Trough. *Marine Geology* **2021,** *437*.

25. Kuhn, T.; Burger, H.; Castradori, D.; Halbach, P., Volcanic and hydrothermal history of ridge segments near the Rodrigues Triple Junction (Central Indian Ocean) deduced from sediment geochemistry. *Marine Geology* **2000,** *169* (3), 391-409.
26. Cave, R. R.; German, C. R.; Thomson, J.; Nesbitt, R. W., Fluxes to sediments underlying the Rainbow hydrothermal plume at 36°14′N on the Mid-Atlantic Ridge. *Geochimica et Cosmochimica Acta* **2002,** *66* (11), 1905-1923.
27. Qiu, Z.; Han, X.; Li, M.; Wang, Y.; Chen, X.; Fan, W.; Zhou, Y.; Cui, R.; Wang, L., The temporal variability of hydrothermal activity of Wocan hydrothermal field, Carlsberg Ridge, northwest Indian Ocean. *Ore Geology Reviews* **2021,** *132*.
28. Shearme, S.; Cronan, D. S.; Rona, P. A., Geochemistry of sediments from the TAG Hydrothermal Field, M.A.R. at latitude 26° N. *Marine Geology* **1983,** *51* (3), 269-291.
29. Liao, S.; Tao, C.; Dias, Á. A.; Su, X.; Yang, Z.; Ni, J.; Liang, J.; Yang, W.; Liu, J.; Li, W.; Dong, C., Surface sediment composition and distribution of hydrothermal derived elements at the Duanqiao-1 hydrothermal field, Southwest Indian Ridge. *Marine Geology* **2019,** *416*.
30. Fan, L.; Wang, G.; Holzheid, A.; Zoheir, B.; Shi, X., Isocubanite-chalcopyrite intergrowths in the Mid-Atlantic Ridge 26°S hydrothermal vent sulfides. *Geochemistry* **2021,** *81* (4).
31. Fan, L.; Wang, G.; Holzheid, A.; Zoheir, B.; Shi, X., Sulfur and copper isotopic composition of seafloor massive sulfides and fluid evolution in the 26°S hydrothermal field, Southern Mid-Atlantic Ridge. *Marine Geology* **2021,** *435*.
32. Fan, L.; Wang, G.; Holzheid, A.; Zoheir, B.; Shi, X.; Lei, Q., Systematic variations in trace element composition of pyrites from the 26°S hydrothermal field, Mid-Atlantic Ridge. *Ore Geology Reviews* **2022,** *148*.
33. Wang, S.; Li, C.; Li, B.; Dang, Y.; Ye, J.; Zhu, Z.; Zhang, L.; Shi, X., Constraints on fluid evolution and growth processes of black smoker chimneys by pyrite geochemistry: A case study of the Tongguan hydrothermal field, South Mid-Atlantic Ridge. *Ore Geology Reviews* **2022,** *140*.
34. Wang, S.; Sun, W.; Huang, J.; Zhai, S.; Li, H., Coupled Fe-S isotope composition of sulfide chimneys dominated by temperature heterogeneity in seafloor hydrothermal systems. *Sci Bull (Beijing)* **2020,** *65* (20), 1767-1774.
35. Tao, C.; Chen, S.; Baker, E. T.; Li, H.; Liang, J.; Liao, S.; Chen, Y. J.; Deng, X.; Zhang, G.; Gu, C.; Wu, J., Hydrothermal plume mapping as a prospecting tool for seafloor sulfide deposits: a case study at the Zouyu-1 and Zouyu-2 hydrothermal fields in the southern Mid-Atlantic Ridge. *Marine Geophysical Research* **2017,** *38* (1), 3-16.
36. Yang, B.; Liu, J.; Li, C.; Zhu, A.; Wang, H.; Cui, J.; Zhang, H.; Hu, Q.; Shi, X., Mineralogical and geochemical characteristics of near-vent metalliferous sediments: Implications for hydrothermal processes along the southern Mid-Atlantic ridge (12°S–28°S). *Ore Geology Reviews* **2022,** *148*.
37. Carbotte, S.; Welch, S. M.; MacDonald, K. C., Spreading rates, rift propagation, and fracture zone offset histories during the past 5 my on the Mid-Atlantic Ridge; 25°–27°30′ S and 31°–34°30′ S. *Marine Geophysical Researches* **1991,** *13* (1), 51-80.
38. James, R. H.; Elderfield, H., Chemistry of ore-forming fluids and mineral formation rates in an active hydrothermal sulfide deposit on the Mid-Atlantic Ridge. *Geology* **1996,** *24* (12), 1147-1150.
39. Niu, Y.; Batiza, R., Magmatic processes at a slow spreading ridge segment: 26°S Mid-Atlantic Ridge. *Journal of Geophysical Research: Solid Earth* **1994,** *99* (B10), 19719-19740.
40. Regelous, M.; Niu, Y.; Abouchami, W.; Castillo, P. R., Shallow origin for South Atlantic Dupal Anomaly from lower continental crust: Geochemical evidence from the Mid-Atlantic Ridge at 26°S. *Lithos* **2009,** *112* (1-2), 57-72.
41. Fan, L.; Wang, G.; Shi, X.; Yang, Y.; Astrid, H.; A, Z. B., Geochemical characteristics and mantle source properties of basalt from the hydrothermal field along the Mid-Atlantic Ridge at 26°S. *Minerology and Petrology* **2020,** *40* (01), 9-20.
42. Shao, M.; Yang, Y.; Su, X.; Ye, J.; Shi, X., Mineralogical Study of Chimneys in the Southern Mid-Atlantic Ridge at 26°S. *China mining magazine* **2014,** *23* (05), 77-81.
43. Dias, Á. S.; Barriga, F. J. A. S., Mineralogy and geochemistry of hydrothermal sediments from the serpentinite-hosted Saldanha hydrothermal field (36°34′N; 33°26′W) at MAR. *Marine Geology* **2006,** *225* (1-4), 157-175.
44. Sun, S.-s.; McDonough, W. F., Chemical and isotopic systematics of oceanic basalts: implications for mantle composition and processes. *Geological Society, London, Special Publications* **1989,** *42* (1), 313-345.
45. Bloemsma, M. R.; Zabel, M.; Stuut, J. B. W.; Tjallingii, R.; Collins, J. A.; Weltje, G. J., Modelling the joint variability of grain size and chemical composition in sediments. *Sedimentary Geology* **2012,** *280*, 135-148.
46. Hannington, M. D.; De Ronde, C. E. J.; Petersen, S.; Hedenquist, J. W.; Thompson, J. F. H.; Goldfarb, R. J.; Richards, J. P., Sea-Floor Tectonics and Submarine Hydrothermal Systems. In *One Hundredth Anniversary Volume*, Society of Economic Geologists: 2005; p 0.

47. Whattam, S. A.; Früh-Green, G. L.; Cannat, M.; De Hoog, J. C. M.; Schwarzenbach, E. M.; Escartin, J.; John, B. E.; Leybourne, M. I.; Williams, M. J.; Rouméjon, S.; Akizawa, N.; Boschi, C.; Harris, M.; Wenzel, K.; McCaig, A.; Weis, D.; Bilenker, L., Geochemistry of serpentinized and multiphase altered Atlantis Massif peridotites (IODP Expedition 357): Petrogenesis and discrimination of melt-rock vs. fluid-rock processes. *Chemical Geology* **2022,** *594*.
48. Mills, R. A.; Elderfield, H., Hydrothermal Activity and the Geochemistry of Metalliferous Sediment. *Geophysical Monograph Series* **1995,** *91*, 392-407.
49. Feely, R. A.; Trefry, J. H.; Lebon, G. T.; German, C. R., The relationship between P/Fe and V/Fe ratios in hydrothermal precipitates and dissolved phosphate in seawater. *Geophysical Research Letters* **1998,** *25* (13), 2253-2256.
50. German, C. R.; Campbell, A. C.; Edmond, J. M., Hydrothermal scavenging at the Mid-Atlantic Ridge: Modification of trace element dissolved fluxes. *Earth and Planetary Science Letters* **1991,** *107* (1), 101-114.
51. Edmonds, H. N.; German, C. R., Particle geochemistry in the Rainbow hydrothermal plume, Mid-Atlantic Ridge. *Geochimica et Cosmochimica Acta* **2004,** *68* (4), 759-772.
52. Mottl, M. J.; McConachy, T. F., Chemical processes in buoyant hydrothermal plumes on the East Pacific Rise near 21°N. *Geochimica et Cosmochimica Acta* **1990,** *54* (7), 1911-1927.
53. German, C. R.; Hergt, J.; Palmer, M. R.; Edmond, J. M., Geochemistry of a hydrothermal sediment core from the OBS vent-field, 21°N East Pacific Rise. *Chemical Geology* **1999,** *155* (1), 65-75.
54. Metz, S.; Trefry, J. H., Field and laboratory studies of metal uptake and release by hydrothermal precipitates. *Journal of Geophysical Research: Solid Earth* **1993,** *98* (B6), 9661-9666.
55. Mills, R. A.; Elderfield, H., Rare earth element geochemistry of hydrothermal deposits from the active TAG Mound, 26°N Mid-Atlantic Ridge. *Geochimica et Cosmochimica Acta* **1995,** *59* (17), 3511-3524.
56. Emerson, S. R.; Huested, S. S., Ocean anoxia and the concentrations of molybdenum and vanadium in seawater. *Marine Chemistry* **1991,** *34* (3), 177-196.
57. Mills, R. A.; Thomson, J.; Elderfield, H.; Hinton, R. W.; Hyslop, E., Uranium enrichment in metalliferous sediments from the Mid-Atlantic Ridge. *Earth and Planetary Science Letters* **1994,** *124* (1), 35-47.
58. Ayupova, N. R.; Melekestseva, I. Y.; Maslennikov, V. V.; Tseluyko, A. S.; Blinov, I. A.; Beltenev, V. E., Uranium accumulation in modern and ancient Fe-oxide sediments: Examples from the Ashadze-2 hydrothermal sulfide field (Mid-Atlantic Ridge) and Yubileynoe massive sulfide deposit (South Urals, Russia). *Sedimentary Geology* **2018,** *367*, 164-174.
59. Hein, J. R.; Clague, D. A.; Koski, R. A.; Embley, R. W.; Dunham, R. E., Metalliferous Sediment and a Silica-Hematite Deposit within the Blanco Fracture Zone, Northeast Pacific. *Marine Georesources & Geotechnology* **2008,** *26* (4), 317-339.
60. Trefry, J. H.; Trocine, R. P.; Klinkhammer, G. P.; Rona, P. A., Iron and copper enrichment of suspended particles in dispersed hydrothermal plumes along the mid-Atlantic Ridge. *Geophysical Research Letters* **1985,** *12* (8), 506-509.
61. Rona, P. A.; Klinkhammer, G.; Nelsen, T. A.; Trefry, J. H.; Elderfield, H., Black smokers, massive sulphides and vent biota at the Mid-Atlantic Ridge. *Nature* **1986,** *321* (6065), 33-37.
62. Rusakov, V. Y.; Shilov, V. V.; Ryzhenko, B. N.; Gablina, I. F.; Roshchina, I. A.; Kuz'mina, T. G.; Kononkova, N. N.; Dobretsova, I. G., Mineralogical and geochemical zoning of sediments at the Semenov cluster of hydrothermal fields, 13°31′-13°30′ N, Mid-Atlantic Ridge. *Geochemistry International* **2013,** *51* (8), 646-669.
63. Cowen, J. P.; Massoth, G. J.; Feely, R. A., Scavenging rates of dissolved manganese in a hydrothermal vent plume. *Deep Sea Research Part A. Oceanographic Research Papers* **1990,** *37* (10), 1619-1637.
64. German, C. R.; Higgs, N. C.; Thomson, J.; Mills, R.; Elderfield, H.; Blusztajn, J.; Fleer, A. P.; Bacon, M. P., A geochemical study of metalliferous sediment from the TAG Hydrothermal Mound, 26°08′N, Mid-Atlantic Ridge. *Journal of Geophysical Research* **1993,** *98* (B6).
65. Dias, Á. S.; Mills, R. A.; Taylor, R. N.; Ferreira, P.; Barriga, F. J. A. S., Geochemistry of a sediment push-core from the Lucky Strike hydrothermal field, Mid-Atlantic Ridge. *Chemical Geology* **2008,** *247* (3-4), 339-351.
66. Popoola, S. O.; Han, X.; Wang, Y.; Qiu, Z.; Ye, Y.; Cai, Y., Mineralogical and Geochemical Signatures of Metalliferous Sediments in Wocan-1 and Wocan-2 Hydrothermal Sites on the Carlsberg Ridge, Indian Ocean. *Minerals* **2019,** *9* (1).